Published in final edited form as:
Proteins. 2015 January ; 83(1): 178–187. doi:10.1002/prot.24722.

Human α-amino-β-carboxymuconate-ε-semialdehyde decarboxylase (ACMSD): A structural and mechanistic unveiling

Lu Huo[†,1], **Fange Liu**[†,1,2], **Hiroaki Iwaki**[§], **Tingfeng Li**[3], **Yoshie Hasegawa**[§], and **Aimin Liu**[†,*]

[†]Departments of Chemistry and the Center for Diagnostics and Therapeutics, Georgia State University, P.O. Box 3965, Atlanta, GA 30303, United States

[§]Department of Life Science and Biotechnology and ORDIST, Kansai University, Suita, Osaka 564-8680, Japan

Abstract

Human α-amino-β-carboxymuconate-ε-semialdehyde decarboxylase determines the fate of tryptophan metabolites in the kynurenine pathway by controlling the quinolinate levels for *de novo* NAD biosynthesis. The unstable nature of its substrate has made gaining insight into its reaction mechanism difficult. Our electron paramagnetic resonance (EPR) spectroscopic study on the catalytically active, Cu-substituted enzyme suggests that the native substrate does not directly ligate to the metal ion. Substrate binding did not result in a change of either the hyperfine structure or the super-hyperfine structure of the EPR spectrum. We also determined the crystal structure of the enzyme in its native state (at 1.99 Å resolution), a substrate analogue-bound form (2.50 Å resolution), and a selected active site mutant form with one of the putative substrate binding residues altered (2.32 Å resolution). These structures illustrate that each asymmetric unit contains 3 pairs of dimers. Consistent with the EPR findings, the ligand-bound complex structure shows that the substrate analogue does not directly coordinate to the metal ion but is bound to the active site by two ariginine residues through non-covalent interactions.

Keywords

Tryptophan metabolites; kynurenine; quinolinate synthesis; quaternary structure

INTRODUCTION

α-Amino-β-carboxymuconate-ε-semialdehyde (ACMS) is a metabolic intermediate found in two catabolic pathways: the kynurenine pathway (Scheme 1), which is responsible for tryptophan catabolism, and the 2-nitrobenzoic acid biodegradation pathway.[1] ACMS is

Correspondence to: Aimin Liu, Department of Chemistry, Georgia State University, 50 Decatur Street, Atlanta, GA 30303, Feradical@gsu.edu.
[1]Both authors contributed equally to this work.
[2]Current address: Department of Chemistry, University of Chicago. Fangel@uchicago.edu
[3]Current address: Division of Basic Pharmaceutics Sciences, Xavier University of Louisiana. tli@xula.edu
[*]This work was supported in whole and in part by the Georgia Research Alliance Distinguished Scientist Program, NSF Grant CHE-1309942, and NIH grant R01GM107529 (A.L.). L.H. acknowledges a fellowship support by the Molecular Basis of Disease Program and a dissertation award from Georgia State University. F.L. acknowledges a University fellowship administrated by the Center for Diagnostics and Therapeutics of Georgia State University. No conflict of interest is declared in this work.

unstable and non-enzymatically dehydrates to quinolinic acid (QUIN) with a $t_{1/2}$ of 33 min at 20 °C, pH 7.0.[2] QUIN is the universal precursor for the *de novo* biosynthesis of NAD, providing the pyridine ring.[3,4] In humans, QUIN levels must be tightly regulated (< 100 nM) because it is also an agonist of *N*-methyl-D-aspartate receptors, and its overproduction can cause overexcitement of neurons and cell death in the central nervous system.[5–9] Elevated QUIN concentrations in bodily fluids have been observed in an exceptionally wide range of neuropsychiatric diseases including anxiety, depression, epilepsy, and neurodegenerative conditions such as Alzheimer's and Huntington's diseases.[5,10–15] A 300-fold elevation of QUIN has also been detected in the brain of patients with HIV infection.[16] Moreover, over the past two decades, an increasingly accumulating volume of evidence unanimously suggest that abnormal activity of the kynurenine pathway participates in the initial phases of neuropathological processes,[13,17] the pathogenesis of AIDS-dementia complex,[18,19] and Alzheimer's disease.[6,10,12,20] When QUIN was injected into healthy rats, the characteristic neuropathological features of Huntington's disease started to develop.[5] Thus, the connection between QUIN and related diseases flows both ways, *i.e*. in symptomatic patients QUIN levels are elevated, and in healthy mammals QUIN injection induces symptoms of disease. Notably, ACMS decarboxylase (ACMSD) directs the vast majority of metabolites to further catabolic steps controlled by enzymes and, by doing so, avoids the overproduction of QUIN (Scheme 1).[1,3] Thus, the decarboxylase ACMSD is of significant biomedical importance.

Prior to this work, the structure of human ACMSD (*h*ACMSD) in its catalytically active form was unavailable. The elucidation of this structural information is crucial for the design of small molecule regulators and for the interpretation of biochemical and spectroscopic studies. We are also interested in the structural and mechanistic divergence between *h*ACMSD from the tryptophan kynurenine pathway and *Pseudomonas fluorescens* (*pf*ACMSD) from the 2-nitrobenzoic acid metabolic pathway. However, *h*ACMSD has proven to be a considerable challenge to express in prokaryotic systems. Although expression of *h*ACMSD as a weakly active enzyme has been achieved in mammalian cell lines[21] and the eukaryote, *Pichia pastoris*,[22] prior attempts to express *h*ACMSD in bacterial systems were all unsuccessful.[21–23]

In the present work, we successfully expressed *h*ACMSD in *E. coli* with the assistance of chaperone co-expression and obtained catalytically active form of the enzyme. By using substrate analogue and metal-substituted *h*ACMSD, we employed a combined structural and spectroscopic approach to tackle the question of how the unstable substrate interacts with the enzyme's active site.

MATERIALS AND METHODS

Expression of Human ACMSD

To construct an N-terminally His_{10}-tagged *h*ACMSD expression plasmid, the *h*ACMSD cDNA,[21] a generous gift from Dr. Fukuoka, was amplified by the polymerase chain reaction with the forward primer 5′-GGAATTCCATATGAAAATTGACATCCATAG-3′ and the reverse primer 5′-CCGCTCGAGTCATTCAAATTGTTTTCTCTC-3′ (built-in *Nde*I and *Xho*I sites are underlined). The PCR product was purified from a 0.8% agarose gel, digested with *Nde*I and *Xho*I, and ligated in the equivalent sites of pET16b (Novagen). After

sequencing, the positive clone was used for transformation into *E. coli* BL21 (DE3) containing the GroEL/ES overexpression plasmid pGro7, pColdII-pGro7, pColdII-pG-Tf2, or pET16b-pG-Tf2, respectively (Takara Corp., Japan).

Cell Culture

Single colonies of *E. coli* containing the appropriate pET-*h*ACMSD plasmid were used to inoculate 50 mL of M9 growth medium (1×M9 medium supplement with 1 mM $MgSO_4$, 0.1 mM $CaCl_2$, 2 μg/mL vitamin B_1, 0.04% casamino acids, 0.4% D-glucose, and a divalent metal ion described below). To obtain *h*ACMSD with desired metal at the active site, a divalent metal ion of either $CoCl_2$, $CuSO_4$, $Fe(NH_4)_2(SO_4)_2$, or $ZnCl_2$ was added to a final concentration of 0.05 to 0.5 mM prior to induce expression. The cell culture medium also contained 100 μg/mL ampicillin, 40 μg/mL chloramphenicol and 500 μg/mL L-arabinose, the latter of which induces the expression of the protein chaperone GroES-GroEL. The cells were grown at 37 °C with shaking until the OD_{600} reached 0.4, at which time the temperature was lowered to 25 °C. *h*ACMSD expression was induced by 0.1 mM isopropyl β-D-thiogalactopyranoside at an OD_{600} of 0.6. The cultures were allowed to further grow at 25 °C for 16 h before being harvested by centrifugation at 8000 × *g* for 15 min at 4 °C. The wet cells were washed with 50 mM potassium phosphate buffer, pH 8.0, twice before storage at −80 °C.

Protein Isolation

Human ACMSD was purified using a modified procedure described for the bacterial analogue.[2] Frozen cells were re-suspended in 50 mM potassium phosphate, pH 8.0, containing 300 mM NaCl and 0.1 mM protease inhibitor phenylmethylsulfonyl fluoride. The cell slurry was passed through an M-110P Microfluidics cell disruptor and the debris was removed by centrifugation at 27,000 × g for 30 min at 4 °C. The supernatant was loaded onto a HiPrep immobilized metal ion affinity chromatography (Ni-NTA) 26/20 column (80 mL resin) for isolation of the native enzyme or FF 16/10 columns charged with either Co^{2+}, Cu^{2+} or Zn^{2+} depending on the corresponding metal-specific *h*ACMSD preparations in order to minimize possible metal cross-contamination in purified protein. The proteins were eluted in a two-step gradient with increased concentration of imidazole in the buffer. The major fractions with ACMSD decarboxylase activity were pooled, concentrated, and further purified on a Superdex 75 column (26/60) using an ÄKTA FPLC protein purification system with a 25 mM HEPES buffer, pH 7.0, containing 5% glycerol. Protein concentrations were determined using Coomassie Plus protein assay reagent (Pierce). The expression level and enzyme purity were determined by SDS-PAGE on 12% polyacrylamide gels.

Metal Analysis

The metal content of ACMSD was assayed in triplicate by inductively coupled plasma optical emission spectrometry (ICP-OES) using a Spectro Genesis spectrometer (Spectro Analytical Instruments GmbH & Co. KG, Germany) as previously described [24]. Metal ions loosely or nonspecifically bound to the enzyme were removed by an overnight incubation of 0.5 mM EDTA with the protein solution at 4 °C followed by desalting on a 5-mL HiTrap

column with 10 mM Tris-HCl (pH 7.4) and buffer wash with the ICP buffer and ultrafiltration.

EPR Spectroscopy

The interaction between ACMS and the enzyme-bound metal center was measured by EPR spectroscopy using Cu-containing ACMSD in the absence or presence of 3 equivalents of ACMS in the assay buffer. The EPR samples were obtained by mixing the protein solution with the substrate solution at 25 °C using a freeze-quenching apparatus, Update Instruments, System 1000. The reaction mixture was shot directly to an EPR tube and frozen in liquid nitrogen. The entire mixing and freezing process was completed in less than 5 seconds. In a parallel EPR experiment, the response of the addition of 3 equivalents of ACMS to copper sulfate was determined with the same buffer system. The same X-band EPR instrumentation is used as those previously described.[1,25]

Steady State Kinetics

The enzyme activity of the recombinant *h*ACMSD was determined according to the procedures described in detail in earlier reports.[1,25,26] Briefly, ACMS was generated from 3-hydroxyanthranilate by an enzymatic method.[1] The ACMSD enzyme assay mixture contained 0 – 120 μM ACMS and an appropriate amount of ACMSD protein in 25 mM HEPES buffer, pH 7.0 with 5% glycerol. Specific activities were calculated from the initial velocities of ACMS decay monitored by the loss of absorption at 360 nm using an absorbance coefficient constant of 47,500 $M^{-1}cm^{-1}$ when the substrate concentration was equal to or lower than 20 μM, or at 320 nm using an absorbance coefficient constant of 9,600 $M^{-1}cm^{-1}$ when the substrate concentration was between 20 – 120 μM. In the enzyme concentration dependence assay, 800 μM Zn-*h*ACMSD was diluted to 200 nM by the reaction buffer. The initial rate of the reaction was monitored from 1 to 240 min frequently in triplet after dilution: a saturated substrate concentration of 15 μM was used.

The inhibition pattern of pyridine-2,6-dicarboxylic acid (PDC) acting on *h*ACMSD was obtained by determining the k_{cat} and K_m in the presence of varying concentrations of PDC (0, 20, 40, and 80 μM) in both buffer and substrate solution. Apparent K_m values for each inhibitor concentration were plotted as a function of inhibitor concentration and inhibition is expressed as K_i values in micromolar (K_i = y-intercept/slope).

X-ray Protein Crystallography

Catalytically active form of Zn-*h*ACMSD was used to screen crystallization conditions in Art Robbins 96-well Intelli-Plates using an ARI Gryphon crystallization robot. The initial hit was obtained from the Index Screening Kit (Hampton Research). After optimization, crystals were obtained from drops assembled with 1.5 μL of 28 mg/mL *h*ACMSD mixed with 1.5 μL of a reservoir solution containing 0.2 M lithium sulfate monohydrate, 0.1 M Tris-HCl pH 6.5 - 7.5, and 20 - 25% polyethylene glycol 3,350, by hanging drop diffusion in VDX plates (Hampton Research). PDC-*h*ACMSD co-crystals were obtained by pre-incubating *h*ACMSD with 10 equivalents of PDC for 30 min prior to crystallization. Crystals suitable for X-ray diffraction were obtained ca. 10 days after crystal growth at 18 °C. Crystallization mother liquor containing 20% glycerol was used as a cryoprotectant. All

crystals obtained under these conditions belong to the $P2_12_12_1$ space group and data were processed with HKL-2000.[27] The three dimensional structures of *h*ACMSD were solved by molecular replacement using our previously published *Pseudomonas fluorescens* (*pf*ACMSD) structure as a search model (PDB code: 2HBV). Molecular replacement and refinement were carried out using PHENIX.[28] Electron density analysis and model building were carried out in Coot.[29] The unit cell images were generated with PyMol[30] with the aid of the SuperSym plugin available at http://supersym.sourceforge.net.

RESULTS

Overexpression of the Human Enzyme in E. coli

*h*ACMSD expressed from the constructed vectors, pColdII-pGro7, pColdII-pG-Tf2, or pET16b-pG-Tf2 was only found in inclusion bodies. Fortunately, the constructed pET16b-pGro7 plasmid expressed *h*ACMSD as a soluble and enzymatically active protein. The enzyme expressed from this system was purified to near homogeneity as described under "Experimental Procedures". Five to ten mg of pure enzyme was obtained from each liter of cell culture when gown in the LB medium; however the yield was significantly reduced when a minimal medium was used. Purified *h*ACMSD is stable at 4 °C for weeks and can endure freeze/thaw cycles with liquid nitrogen multiple times without a significant loss of activity.

Metal Content and Catalytic Activity

Metal analysis of *h*ACMSD purified from cells grown in the LB medium contained several metals. Iron, zinc and copper were present and the total metal content was substoichiometric (Table 1). Metal analysis of *h*ACMSD purified from the cells cultured in the M9 minimal media supplemented with 100 μM of varying metal ions is presented in Table 1. Activity assays demonstrated that *h*ACMSD expressed in the presence of Zn^{2+} exhibited activity comparable to what was found for the most active forms of *pf*ACMSD bound with a Zn^{2+} or Co^{2+} ion.[19] Co^{2+}-containing *h*ACMSD, on the other hand, exhibited very little specific enzymatic activity relative to Co-*pf*ACMSD. It should be noted that the contribution of Zn ion to the activity of Co-, Cu-, and Fe-*h*ACMSD was subtracted based on the metal analysis data (Table 1) with regard to the Zn-*h*ACMSD activity.

Unlike *pf*ACMSD,[1] the metal ions in *h*ACMSD could not be removed by the metal chelators EDTA, 1,10-phenanthroline or 8-hydroxy-quinoline-5-sulfonic acid, and the enzyme activity was not affected by the addition of these metal chelators. Moreover, the addition of one to ten equivalents of Co^{2+}, Cu^{2+}, Fe^{2+}, or Zn^{2+} to purified *h*ACMSD did not increase enzyme activity, indicating that the purified human enzyme cannot be reconstituted *in vitro*.

Since *in vitro* metal reconstitution was not successful for the human enzyme, we attempted to add zinc ions to the M9 medium at various concentrations prior to induction of the cells. The enzyme isolated in this set of experiments contained different amount of naturally incorporated zinc ion during protein synthesis. Fig. 1 shows that the activity of *h*ACMSD is proportional to the zinc content of the enzyme. These results suggest that *h*ACMSD is a zinc-dependent metalloenzyme. Zn-*h*ACMSD yielded steady-state kinetic parameters

similar to those of Zn^{2+}-containing *pf*ACMSD.[31] A k_{cat} value of 4.8 s^{-1} was measured for *h*ACMSD with 64.4% zinc ion occupancy. This value is anticipated to be 7.5 s^{-1} with a fully-loaded zinc ion. The K_m (5.8 μM) and the k_{cat} (7.5 s^{-1}) values of *h*ACMSD are comparable to the K_m (9.6 μM) and the k_{cat} (6.5 s^{-1}) reported for Zn-*pf*ACMSD with *ca.* 80% zinc occupancy.[31]

When *h*ACMSD was diluted from 800 μM to 200 nM, it lost 90% of activity after 4 h (Fig. 2). Since proteins prefer to form higher oligomer state at higher concentration, the *h*ACMSD dimer will start to dissociate once its concentration drops. Losing catalytic activity after dilution implies that *h*ACMSD is unlikely to be active in the monomeric state. Similar observations have been reported for the bacterial ACMSD.[26]

Probing the Nature of the Enzyme-Substrate Interactions

Although ACMS is an unstable molecule, we find that it tends to form stable complexes with various metal ions. Because Zn^{2+} is EPR silent while Cu^{2+} is EPR active with well refined hyperfine signals sensitive to X-band EPR, copper substituted ACMSD is used in this section of experiment. Fig. 3(A) shows that ACMS binds to a cupric ion in solution. The EPR signal intensity of $CuSO_4$ solution is weak due to the coupling of copper ions. Addition of unstable ACMS to $CuSO_4$ led to the formation of stable Cu^{2+}-ACMS complex which gives rise to well-resolved type II copper EPR spectrum.[32] Since this technique is highly sensitive to the changes of the electronic/chemical structure of a Cu^{2+} ion, especially when the superhyperfine structure is resolved, we analyzed ACMS perturbation to the enzyme-bound copper center by EPR spectroscopy.

To probe whether the substrate ACMS is ligated directly to the metal, we obtained Cu-substituted *h*ACMSD. Since the metal ion cannot be extracted and reconstituted, we circumvented this problem by isolating the human enzyme from cell culture of a metal-depleted minimal medium supplemented with cupric ion. The Cu-substituted protein is catalytically active although it is a relatively poor catalyst. Its k_{cat} value was 0.1 ± 0.02 s^{-1} and K_m value was 3.3 ± 0.2 μM.

Both hyperfine splitting due to the nuclear spin of copper (I = 3/2) and nitrogen (I = 1)-induced superhyperfine interactions are present in the EPR spectrum of Cu-*h*ACMSD [Figure 2(B)]. The EPR parameters obtained from a simulation of the spectrum of wild-type Cu-*h*ACMSD have an $A_{//}$ value of 18.7 mT and a $g_{//}$ value of 2.218, both typical for a type II Cu^{2+} center. In the perpendicular region, a multiple-line superhyperfine structure with a splitting of about 1.5 mT is well resolved in the spectrum [Fig. 3(C)]. The superhyperfine structure originates from the spin-spin interaction between the nuclear spin of the nitrogen atoms (nuclear spin I = 1) and the electron spin of the Cu^{2+} ion. When 3 molar equivalents of ACMS were added to Cu-*h*ACMSD, frozen in less than 5 s, and subsequently measured by EPR at 20 K, no spectral change was observed. In sharp contrast to the free copper ion in solution, the presence of ACMS is unable to induce any disturbance in the hyperfine and superhypefine structures of the Cu center in *h*ACMSD. Thus, there is no direct ligation between ACMS and the Cu center in the enzyme.

Crystal Structure

The structure of *h*ACMSD was obtained from native, catalytically competent form of the enzyme and was refined to 1.99 Å resolution (Table 2, PDB entry: 4OFC). Each unit cell contains four asymmetric units in which six protomers are found as a trimer of dimer, as shown in Fig. 4. The dimer interface contains a surface area of about 2,400–2,460 $Å^2$ and is primarily formed by three helical regions which are composed of residues 191 to 201, 230 to 244, and 271 to 281 of each subunit. The central area of the dimer interface is strictly hydrophobic. Analysis of the dimer interface reveals a total of 24–33 direct hydrogen bonding interactions and 18–21 salt bridges for each dimer.

Due to the instability of ACMS, the substrate-bound ACMSD structure is not yet available. However, pyridine-2,6-dicarboxylic acid is a heterocyclic, stable ACMS analogue that competitively inhibits the bacteria ACMSD.[26] We found that it is also an effective competitive inhibitor of *h*ACMSD [Fig. 5(A)] with a K_i value of 15.2 ± 0.5 μM. We successfully co-crystallized this compound with *h*ACMSD (Table 2, PDB entry: 4IH3) and the overall structure is nearly identical to the ligand-free enzyme. PDC is bound at the active site and forms ionic interactions with Arg47 and Arg235*, where the asterisk indicates this residue is from a neighboring subunit [Fig. 5(B)]. The PDC-bound structure shows that the inhibitor is fairly close to the zinc ion with the C4 *ca*. 2.6 Å from the zinc ion. However, the closest oxygen is 5.6 Å away from the metal ion. Thus, the substrate analogue does not directly coordinate to the metal ion.

To further prove that the unstable substrate binds to the enzyme by the active site arginines, we mutated Arg47 and Arg235* to alanine. Both R47A and R235A variants showed no detectable catalytic activity, proving that they are important residues for catalysis. The result of this analysis is consistent with our structural findings shown in Fig. 4(B). While R235A eludes crystallization, the crystal structure of the R47A mutant was solved at 2.32 Å resolution (Table 2). Similar to the wild-type enzyme structure, six protomers in three dimers are present in each asymmetric unit. The same interface region is observed between the protomers as observed in the wild-type enzyme. The RMSD value is only 0.254 Å from 14,034 out of 14,040 atoms for the structures of R47A and wild type.

DISCUSSION

Our work on human ACMSD solved several long-standing mysteries. The first pertains to the cofactor identity. Our previous work on the analogous bacterial system indicates that *pf*ACMSD is a metal-dependent enzyme.[1,25,31] Thus, one would expect *h*ACMSD is a metalloprotein. However, all prior studies on *h*ACMSD suggest that the catalytic activity of human enzyme is independent of metal ions.[21,22] This is likely due to the observation that neither a metal chelator, nor external metal affects the activity of purified *h*ACMSD. The first crystal structure of *h*ACMSD was later determined with a zinc ion bound at the enzyme active site, but how the zinc ion is associated with catalytic activity was not discussed,[23] leaving a questionable cofactor-free conclusion for *h*ACMSD in literature. Here, by showing protein expressed in a minimal medium supplemented with increasing concentrations of zinc ions, giving higher decarboxylase activity together with the data present in Table 1, we found that the zinc enzyme presents the highest catalytic activity. The catalytic efficiency of

Zn-*h*ACMSD is significantly higher than that previously reported for the same enzyme expressed in *Pichia pastoris*, which has a similar K_m but a lower k_{cat} value of 1.0 s^{-1}.[22] Thus, it becomes evident that the *h*ACMSD is a zinc-dependent enzyme.

Since metal chelators are demonstrated to be able to extract the metal ion from *pf*ACMSD but not *h*ACMSD, *h*ACMSD apparently binds its metal more tightly. The crystal structures solved provide a molecular understanding for this nonconformity. An aspartate and three histidine residues in *h*ACMSD coordinate the zinc ion. Notably, His174 is a metal ligand in all six protomers of each asymmetric unit of the structure, with a bond distance of 2.2–2.3 Å. In contrast, the equivalent histidine in *pf*ACMSD, His177, presents significant flexibility in the structure we have solved (PDB entry: 2HBV). In subunit A, His177 coordinate to the zinc ion with distance of 2.2 Å. In subunit B, His177 is no longer a metal ligand and is 4.2 Å away from the zinc ion. Thus, His177 is a weaker ligand in *pf*ACMSD. The observed metal affinity deviation therefore becomes understood.

It is challenging to predict the cofactor dependency of a protein base on the primary structure if the cofactor is a single atomic metal. Although characteristic sequences can be used to identify some metal binding motifs, including zinc finger, calcium EF hand, and iron-sulfur cluster, drawing conclusions based solely on sequence can be misleading. For example, LigI is a member of the amidohydrolase superfamily, whose members were all previously demonstrated to be divalent metal dependent including ACMSD. Based on sequence alignment, LigI has all four conserved residues, three histidines and one aspartate, for metal coordination. However, later mechanistic and structural studies revealed that LigI is actually metal independent and the four metal ligand residues are with new catalytic roles.[33] Sometimes, even with the assistance of biochemical study, prediction of metal cofactor can still be misjudged. The enzyme uronate isomerase catalyzes the isomerization reaction of D-glucuronate and D-fructuronate was initially thought to be metal independent because metal chelators do not affect the enzyme activity.[4] Later on, an improved study suggested that uronate isomerase is actually a mononuclear zinc-containing enzyme.[34] Hence, a combined knowledge of sequence, biochemical assay, and structure is needed to correctly identify a metal cofactor.

Since its initial identification from rat liver, ACMSD has been known for 58 years[35] and this enzyme has arisen significant biomedical interest. Following our success in obtaining the bacterial enzyme structure in 2006,[31] a structure of the enzyme in its inactive form, complexed with 1,3-dihydroxyacetone-phosphate (DHAP), was obtained through molecular replacement in 2009 by Garavaglia et al. (PDB entry 2WM1).[23] It should be noted that the DHAP-bound structure is monomeric with only one subunit in each asymmetry unit, whereas the three *h*ACMSD structures present in this study, including a substrate-free and ligand-bound structure, and all of the *pf*ACMSD structures determined thus far,[24,26,31] are homodimers.

A quaternary structure variety is apparently present in the structural studies of *h*ACMSD. We think that the diversity brings up the following questions: (1) is the quaternary structure of ACMSD linked to the catalytic activity, and (2) is a ligand-induced structural change a potential mechanism of catalytic activity regulation? While the latter question will be a

subject for future study, the results presented in this work and the comparison with our previous studies on the bacterial enzyme shed insightful clues, as discussed below.

We have recently shown that *pf*ACMSD is a mixture of monomer and dimer in solution, and that the former is catalytically inactive while the latter is functionally competent.[26] The decarboxylase activity is dependent on the presence of two arginine residues (Arg51 and Arg239*, star indicates that Arg239 is from the neighboring subunit), which play a key role in substrate binding [26]. Likewise, when *h*ACMSD is in the dimeric form, the conserved arginine residues (Arg47 and Arg235*) are both present in the active site in a manner resembling what has been described for *pf*ACMSD (Fig. 6). When *h*ACMSD is in the monomeric form bound with the DHAP, Arg235 is 25 Å from the catalytic metal and cannot be a residue involved in substrate binding.[23] Thus, these conserved arginine residues are effective probes for determining the functional assembly of ACMSD.

The enzyme 5-carboxyl-uracil decarboxylase (IDCase) is a member of the ACMSD subfamily under the amidohydrolase superfamily and has very high sequence similarity to ACMSD.[36,37] This enzyme is the most closely related neighbor of ACMSD in the reconstructed evolution tree. Recently, the overall structures of IDCase from both *Cordyceps militaris* and *Metarhizium anisopliae* mostly resemble the structure of ACMSD.[38] Interestingly, in both of the substrate 5-carboxyl-uracil and inhibitor 5-nitro-uracil bound binary complex structures, the catalytic metal ion does not directly interact with the substrate and inhibitor. The two conserved arginine residues, Arg68 (equivalent to Arg47 of *h*ACMSD) and Arg262* (equivalent to Arg235* of *h*ACMSD) from the neighboring subunit play major roles in substrate/inhibitor binding. Specifically, Arg262* binds to the leaving carboxyl group in the substrate bound structure (PDB entry: 4LAM). This observation further suggests that Arg47 and Arg235* are responsible for substrate binding not only in ACMSD but also in proteins from the same subfamily. As a result, a dimeric quaternary structure is most likely required for enzyme activity through the ACMSD subfamily.

Since mammals have no mechanism to store free amino acids not used for protein synthesis, tryptophan is primarily directed towards catabolism. During starvation, when tryptophan levels are low, the priority of catabolism is to preserve the kynurenine pathway intermediates for NAD biosynthesis and thus, the activity of ACMSD must be lessened. Using a glycolic intermediate, DHAP, to force ACMSD to change its structure to the catalytically inactive monomeric form is a possibly unprecedented metabolic interrelation between the tryptophan kynurenine catabolic pathway and glycolysis.

CONCLUSION

The biochemical, spectroscopic, and structural results led us to conclude that *h*ACMSD is a zinc-dependent dimeric enzyme that harnesses its unstable, negatively charged substrate by its two positively charged residues rather than by the metal ion during substrate positioning at the early stage of the catalytic cycle. The quaternary structure variety, previously demonstrated in the bacterial analogous enzyme[26] and now implicated in the human enzyme, is directly linked to the enzyme catalytic activity. Thus, the structural arrangement

of the catalytic center offers a potential regulatory mechanism at a critical junction of the downstream tryptophan kynurenine pathway.

Acknowledgments

We thank Dr. Shin-Ichi Fukuoka for providing cDNA clone of human ACMSD, Dr. Lirong Chen and Dr. Ezra Peisach for stimulating discussions in the analyses of the structural data, and Ian Davis for critical discussion.

Abbreviations

QUIN	quinolinate or quinolinic acid
ACMS	α-amino-β-carboxymuconate-ε-semialdehyde
ACMSD	ACMS decarboxylase
DHAP	1,3-dihydroxyacetone-phosphate
IDCase	5-carboxyl-uracil decarboxylase
PDC	pyridine-2,6-dicarboxylic acid

References

1. Li T, Walker AL, Iwaki H, Hasegawa Y, Liu A. Kinetic and spectroscopic characterization of ACMSD from *Pseudomonas fluorescens* reveals a pentacoordinate mononuclear metallocofactor. J Am Chem Soc. 2005; 127:12282–12290. [PubMed: 16131206]
2. Li T, Ma J, Hosler JP, Davidson VL, Liu A. Detection of transient intermediates in the metal-dependent non-oxidative decarboxylation catalyzed by α-amino-β-carboxymuconic-ε-semialdehyde decarboxylase. J Am Chem Soc. 2007; 129(30):9278–9279. [PubMed: 17625866]
3. Colabroy KL, Begley TP. The pyridine ring of NAD is formed by a nonenzymatic pericyclic reaction. J Am Chem Soc. 2005; 127(3):840–841. [PubMed: 15656614]
4. Williams L, Nguyen T, Li Y, Porter TN, Raushel FM. Uronate isomerase: a nonhydrolytic member of the amidohydrolase superfamily with an ambivalent requirement for a divalent metal ion. Biochemistry. 2006; 45(24):7453–7462. [PubMed: 16768441]
5. Schwarcz R, Whetsell WO Jr, Mangano RM. Quinolinic acid: an endogenous metabolite that produces axon-sparing lesions in rat brain. Science. 1983; 219(4582):316–318. [PubMed: 6849138]
6. Stone TW, Darlington LG. Endogenous kynurenines as targets for drug discovery and development. Nat Rev Drug Discov. 2002; 1(8):609–620. [PubMed: 12402501]
7. Schwarcz R, Guidetti P, Sathyasaikumar KV, Muchowski PJ. Of mice, rats and men: revisiting the quinolinic acid hypothesis of Huntington's disease. Prog Neurobiol. 2010; 90(2):230–245. [PubMed: 19394403]
8. Lahdou I, Sadeghi M, Oweira H, Fusch G, Daniel V, Mehrabi A, Jung G, Elhadedy H, Schmidt J, Sandra-Petrescu F, Iancu M, Opelz G, Terness P, Schefold JC. Increased serum levels of quinolinic acid indicate enhanced severity of hepatic dysfunction in patients with liver cirrhosis. Hum Immunol. 2013; 74(1):60–66. [PubMed: 23046794]
9. Owe-Young R, Webster NL, Mukhtar M, Pomerantz RJ, Smythe G, Walker D, Armati PJ, Crowe SM, Brew BJ. Kynurenine pathway metabolism in human blood-brain-barrier cells: implications for immune tolerance and neurotoxicity. J Neurochem. 2008; 105(4):1346–1357. [PubMed: 18221377]
10. Baran H, Jellinger K, Deecke L. Kynurenine metabolism in Alzheimer's disease. J Neural Transm. 1999; 106(2):165–181. [PubMed: 10226937]
11. Beal MF, Ferrante RJ, Swartz KJ, Kowall NW. Chronic quinolinic acid lesions in rats closely resemble Huntington's disease. J Neurosci. 1991; 11(6):1649–1659. [PubMed: 1710657]

12. Stone TW, Behan WM, Jones PA, Darlington LG, Smith RA. The role of kynurenines in the production of neuronal death, and the neuroprotective effect of purines. J Alzheimers Dis. 2001; 3(4):355–366. [PubMed: 12214038]
13. Stone TW, Mackay GM, Forrest CM, Clark CJ, Darlington LG. Tryptophan metabolites and brain disorders. Clin Chem Lab Med. 2003; 41(7):852–859. [PubMed: 12940508]
14. Guillemin GJ, Williams KR, Smith DG, Smythe GA, Croitoru-Lamoury J, Brew BJ. Quinolinic acid in the pathogenesis of alzheimer's disease. Adv Exp Med Biol. 2003; 527:167–176. [PubMed: 15206729]
15. Guidetti P, Schwarcz R. 3-Hydroxykynurenine and quinolinate: pathogenic synergism in early grade huntington's disease? Adv Exp Med Biol. 2003; 527:137–145. [PubMed: 15206726]
16. Heyes MP, Saito K, Lackner A, Wiley CA, Achim CL, Markey SP. Sources of the neurotoxin quinolinic acid in the brain of HIV-1-infected patients and retrovirus-infected macaques. FASEB J. 1998; 12(10):881–896. [PubMed: 9657528]
17. Schwarcz R. The kynurenine pathway of tryptophan degradation as a drug target. Curr Opin Pharmacol. 2004; 4(1):12–17. [PubMed: 15018833]
18. Guillemin GJ, Kerr SJ, Brew BJ. Involvement of quinolinic acid in AIDS dementia complex. Neurotox Res. 2005; 7(1–2):103–123. [PubMed: 15639803]
19. Guillemin GJ, Wang L, Brew BJ. Quinolinic acid selectively induces apoptosis of human astrocytes: potential role in AIDS dementia complex. J Neuroinflammation. 2005; 2:16. [PubMed: 16042813]
20. Widner B, Leblhuber F, Walli J, Tilz GP, Demel U, Fuchs D. Tryptophan degradation and immune activation in Alzheimer's disease. J Neural Transm. 2000; 107(3):343–353. [PubMed: 10821443]
21. Fukuoka S, Ishiguro K, Yanagihara K, Tanabe A, Egashira Y, Sanada H, Shibata K. Identification and expression of a cDNA encoding human α-amino-β-carboxymuconic-ε-semialdehyde decarboxylase (ACMSD). A key enzyme for the tryptophan-niacine pathway and "quinolinate hypothesis". J Biol Chem. 2002; 277(38):35162–35167. [PubMed: 12140278]
22. Pucci L, Perozzi S, Cimadamore F, Orsomando G, Raffaelli N. Tissue expression and biochemical characterization of human α-amino-β-carboxymuconic-ε-semialdehyde decarboxylase, a key enzyme in tryptophan catabolism. FEBS J. 2007; 274(3):827–840. [PubMed: 17288562]
23. Garavaglia S, Perozzi S, Galeazzi L, Raffaelli N, Rizzi M. The crystal structure of human α-aminoβ-carboxymuconic-ε-semialdehyde decarboxylase in complex with 1,3-dihydroxyacetonephosphate suggests a regulatory link between NAD synthesis and glycolysis. FEBS J. 2009; 276(22):6615–6623. [PubMed: 19843166]
24. Huo L, Fielding AJ, Chen Y, Li T, Iwaki H, Hosler JP, Chen L, Hasegawa Y, Que L Jr, Liu A. Evidence for a dual role of an active site histidine in α-amino-β-carboxymuconic-ε-semialdehyde decarboxylase. Biochemistry. 2012; 51(29):5811–5821. [PubMed: 22746257]
25. Li T, Iwaki H, Fu R, Hasegawa Y, Zhang H, Liu A. α-amino-β-carboxymuconic-ε-semialdehyde decarboxylase (ACMSD) is a new member of the amidohydrolase superfamily. Biochemistry. 2006; 45(21):6628–6634. [PubMed: 16716073]
26. Huo L, Davis I, Chen L, Liu A. The power of two: arginine 51 and arginine 239* from a neighboring subunit are essential for catalysis in α-amino-β-carboxymuconic-ε-semialdehyde decarboxylase. J Biol Chem. 2013; 288(43):30862–30871. [PubMed: 24019523]
27. Otwinowski Z, Minor W. Processing of X-ray diffraction data collected in oscillation mode. Method Enzymol. 1997; 276:307–326.
28. Adams PD, Afonine PV, Bunkoczi G, Chen VB, Davis IW, Echols N, Headd JJ, Hung LW, Kapral GJ, Grosse-Kunstleve RW, McCoy AJ, Moriarty NW, Oeffner R, Read RJ, Richardson DC, Richardson JS, Terwilliger TC, Zwart PH. PHENIX: a comprehensive Python-based system for macromolecular structure solution. Acta Crystallogr D Biol Crystallogr. 2010; 66(Pt 2):213–221. [PubMed: 20124702]
29. Emsley P, Cowtan K. Coot: model-building tools for molecular graphics. Acta Crystallogr D Biol Crystallogr. 2004; 60:2126–2132. [PubMed: 15572765]
30. The PyMOL Molecular Graphics System, Version 1504. Schrödinger, LLC; www.pymol.org
31. Martynowski D, Eyobo Y, Li T, Yang K, Liu A, Zhang H. Crystal structure of α-amino-β-carboxymuconic-ε-semialdehyde decarboxylase (ACMSD): insight into the active site and

catalytic mechanism of a novel decarboxylation reaction. Biochemistry. 2006; 45:10412–10421. [PubMed: 16939194]

32. Howes BD, Abraham ZH, Lowe DJ, Bruser T, Eady RR, Smith BE. EPR and electron nuclear double resonance (ENDOR) studies show nitrite binding to the type 2 copper centers of the dissimilatory nitrite reductase of Alcaligenes xylosoxidans (NCIMB 11015). Biochemistry. 1994; 33(11):3171–3177. [PubMed: 8136351]
33. Hobbs ME, Malashkevich V, Williams HJ, Xu C, Sauder JM, Burley SK, Almo SC, Raushel FM. Structure and catalytic mechanism of LigI: insight into the amidohydrolase enzymes of cog3618 and lignin degradation. Biochemistry. 2012; 51(16):3497–3507. [PubMed: 22475079]
34. Nguyen TT, Fedorov AA, Williams L, Fedorov EV, Li Y, Xu C, Almo SC, Raushel FM. The mechanism of the reaction catalyzed by uronate isomerase illustrates how an isomerase may have evolved from a hydrolase within the amidohydrolase superfamily. Biochemistry. 2009; 48(37): 8879–8890. [PubMed: 19678710]
35. Mehler AH. Formation of picolinic and quinolinic acids following enzymatic oxidation of 3-hydroxyanthranilic acid. J Biol Chem. 1956; 218(1):241–254. [PubMed: 13278331]
36. Liu, A.; Li, T.; Fu, R. Amidohydrolase Superfamily. John Wiley & Sons Ltd; 2007.
37. Liu A, Zhang H. Transition metal-catalyzed nonoxidative decarboxylation reactions. Biochemistry. 2006; 45(35):10407–10411. [PubMed: 16939193]
38. Xu S, Li W, Zhu J, Wang R, Li Z, Xu GL, Ding J. Crystal structures of isoorotate decarboxylases reveal a novel catalytic mechanism of 5-carboxyl-uracil decarboxylation and shed light on the search for DNA decarboxylase. Cell Res. 2013; 23(11):1296–1309. [PubMed: 23917530]

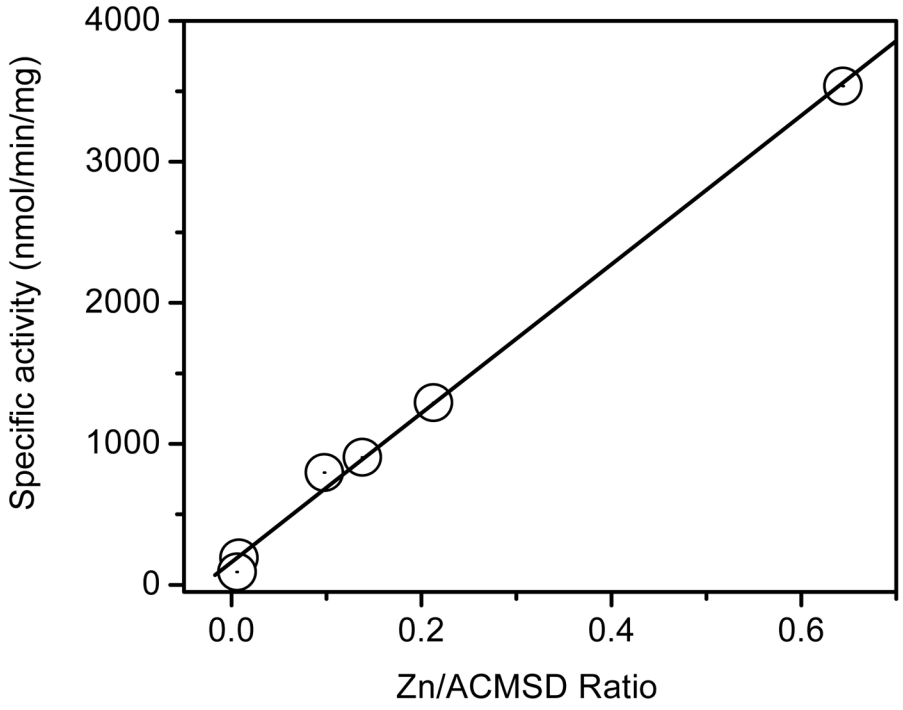

Figure 1.

The specific catalytic activity of *h*ACMSD as a function of Zn content in the protein. The variation of Zn content was achieved by growing cells in M9 minimum medium supplemented with 0 – 500 μM concentrations of $ZnCl_2$.

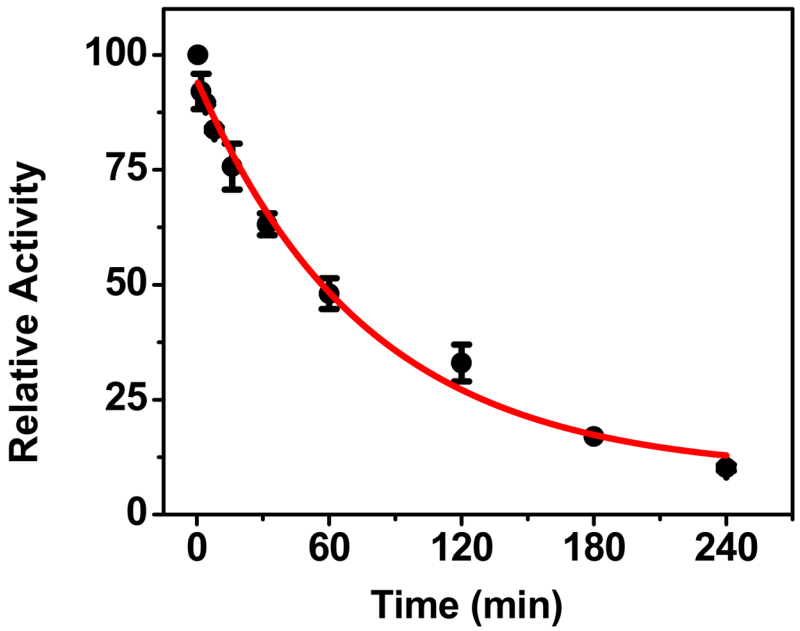

Figure 2.

The catalytic activity of *h*ACMSD decays after dilution, indicating that *h*ACMSD has better activity at higher oligomerization state. The relative activity of concentrated and diluted samples was measured under the same conditions as described in the text. The experimental data was fitted with first exponential decay (red line).

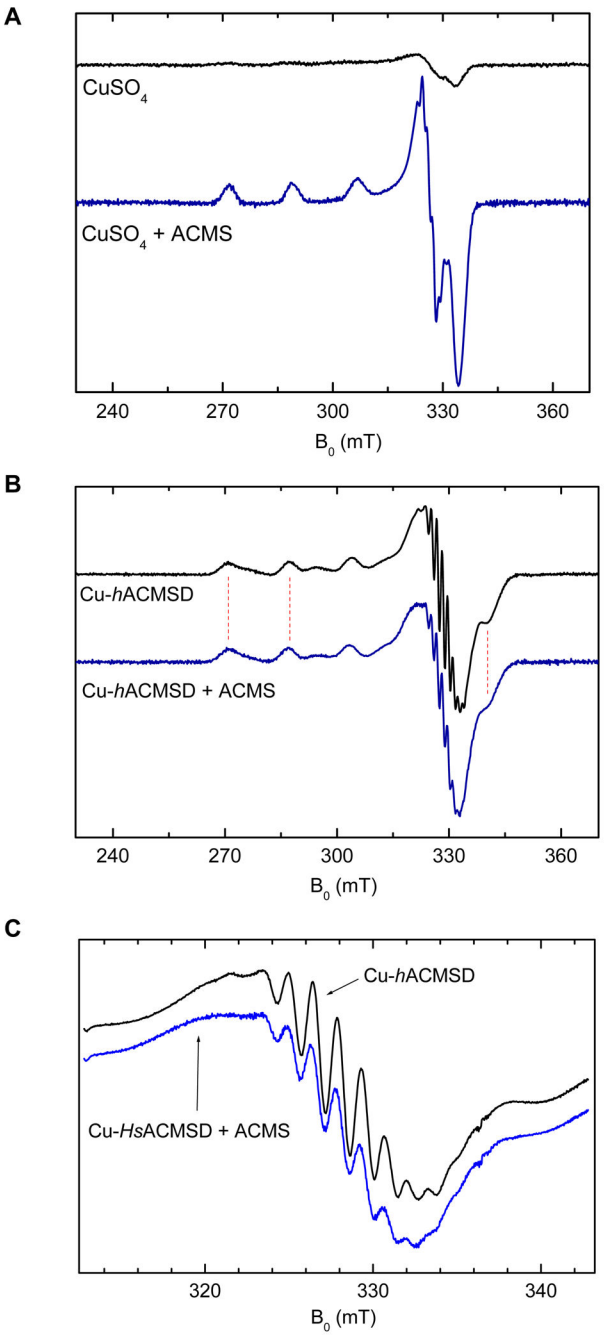

Figure 3.

Low-temperature X-band EPR spectroscopic study confirms that the substrate binds to the free metal ion but does not directly coordinate to the catalytic metal ion in ACMSD. (**A**) Free $CuSO_4$ and $CuSO_4$-ACMS (1:3) at 200 μM concentration, (**B**) as-isolated Cu-*h*ACMSD (200 μM) and Cu-*h*ACMSD-ACMS (1:3), and (**C**) a magnified view of superhyperfine structure of Cu-*h*ACMSD in the absence/presence of ACMS (600 μM). The spectrometer conditions: temperature, 20 K; modulation amplitude, 0.3 mT; microwave

power, 0.5 mW; time constant, 40.96 ms; and sweep time 1.79 mT/s for the field from 225 to 375 mT.

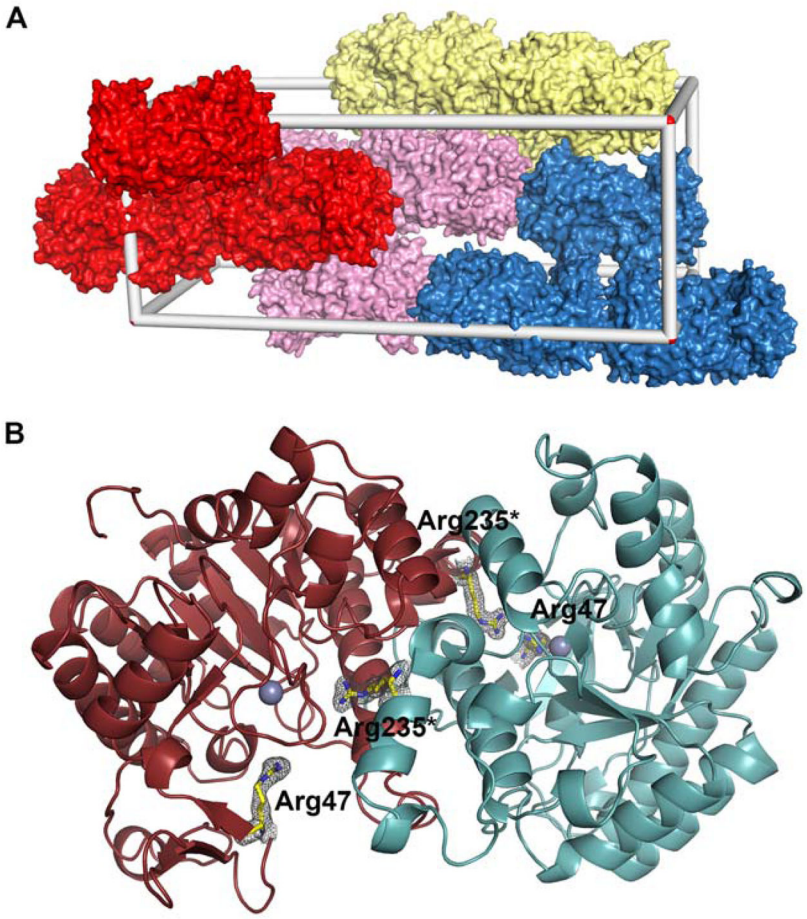

Figure 4.

The crystal structure of *h*ACMSD is solved as a homodimer with a zinc ion bound at the catalytic center. (**A**) Each unit cell contains 4 asymmetric units of 3 pairs of dimers. (**B**) The catalytic center contains two arginine residues, Arg47 and Arg235*. Star indicates Arg235 is from a neighboring subunit.

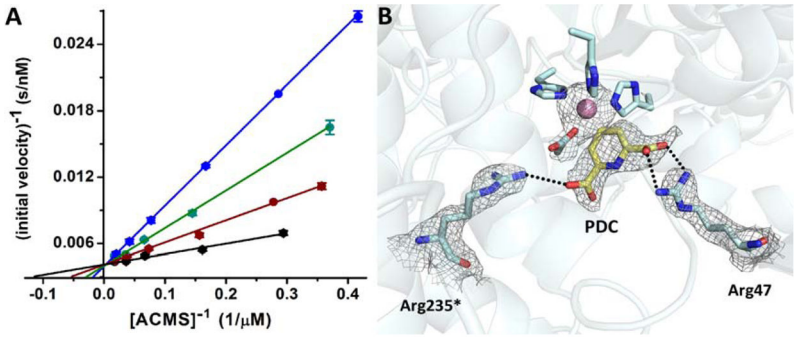

Figure 5.

The crystal structure of *h*ACMSD in complex with a substrate analogue sheds light on the enzyme-substrate interaction mode. (**A**) Competitive inhibition of *h*ACMSD by 0, 20, 40, and 80 μM of pyridine-2,6-dicarboxylic acid (PDC) as the black, red, green, and blue traces, respectively. (**B**) The co-crystalized structure shows that the competitive inhibitor PDC is bound by Arg47 (right Arg in the figure) and Arg235* (left) near the zinc ion (pink ball).

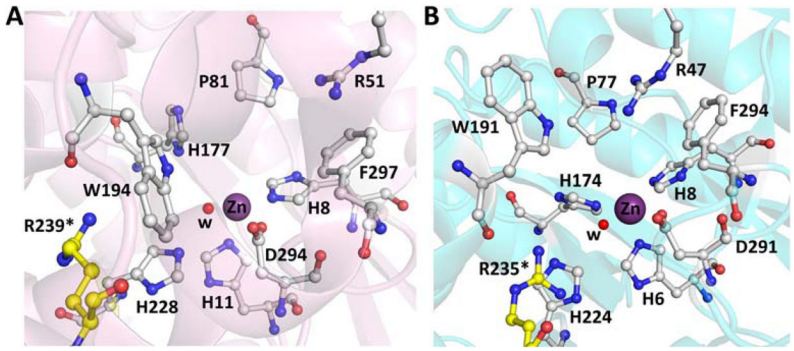

Figure 6.

A side-by-side comparison of the active site architecture of (**A**) *pf*ACMSD and (**B**) *h*ACMSD shows similar substrate binding environment. Two arginine residues, including one from the neighboring subunit (with its carbon atoms highlighted in yellow), must be present in the active site for the decarboxylase activity.

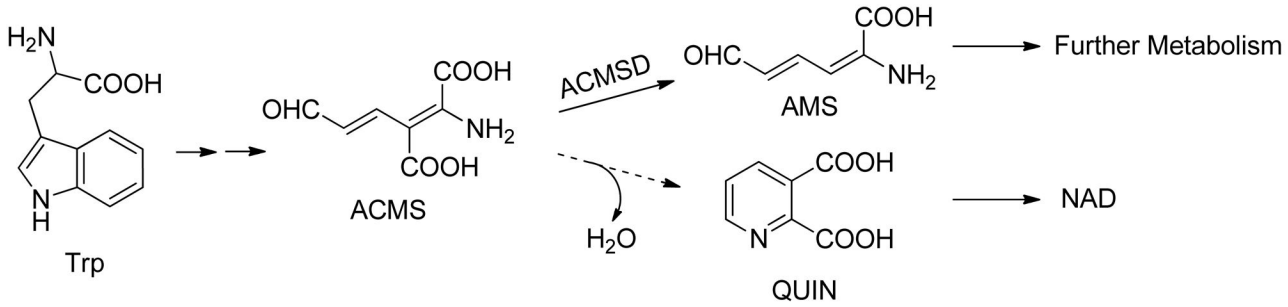

Scheme 1.

ACMSD competes with a non-enzymatic spontaneous cyclic reaction (marked with dotted arrow) and directs the vast majority of ACMS to enzyme-mediated catabolic pathway.

Table 1

Percentage of metal occupation and corresponding activity of *h*ACMSD from different medium cultures.

	LB	**M9**	**M9 + Co^{2+}**	**M9 + Cu^{2+}**	**M9 + Fe^{2+}**	**M9 + Zn^{2+}**
Co	0	0	96.8	0.4	0.8	0
Cu	2.2	2.9	0.7	47.9	3.6	9.7
Fe	28.7	9.8	1.0	10.0	55.1	7.5
Zn	13.8	9.8	0.8	0.6	7.7	64.4
Specific activity (nmol/min/mg)	910	800	234* 190	123* 90	823* 400	3540

The metal ions of *h*ACMSD were incorporated into the enzyme during protein assembly. Metal content was measured as described in Experimental Procedures. The concentration of the metal ions supplemented to the M9 medium was 0.1 mM in each of the above experiments. The values were the average numbers of three independent experiments with standard deviation smaller than 5%.

* indicating data prior to subtracting the contribution of Zn ion.

Table 2

X-ray crystallography data collection and refinement statistics

Data collection	*h*ACMSD	PDC-*h*ACMSD	R47A *h*ACMSD
Space group	$P2_12_12_1$	$P2_12_12_1$	$P2_12_12_1$
Unit cell lengths (Å)	a=88.704, b=101.082, c=232.820	a=88.368, b=101.655, c=233.117	a=89.142, b=101.686, c=232.613
Unit cell angles (°)	α=γ=β=90	α=γ=β=90	α=β=γ=90
Wavelength (Å)	1.0	1.0	0.8
Temperature (K)	100	100	100
Resolution (Å)[a]	45.00–1.96 (2.03–1.99)	45.00–2.50 (2.50–2.54)	50.00–2.33 (2.37–2.33)
Completeness (%)[a]	87.6 (81.3)	75.4 (65.7)	98.4 (82.8)
R_{merge} (%)[a, b]	15.3 (78.2)	9.9 (29.3)	13.2 (48.6)
$I/\sigma I$ [a]	20.6 (2.3)	10.3 (1.5)	17.9 (2.0)
Multiplicity [a]	10.1 (8.0)	9.7 (8.5)	25.3 (13.7)
Refinement			
Resolution (Å)	1.96	2.49	2.32
No. reflections; working/test	130135/6497	55192/2809	85220/4492
R_{work} (%)[c]	19.9	23.3	20.8
R_{free} (%)[d]	24.1	29.8	27.6
No. of protein atoms	15984	15810	15774
No. of ligand atoms	6	78	6
No. of solvent sites	994	286	821
Average B factor (Å^2)			
Protein	29.7	33.3	30.0
Zn(II) or PDC	26.3	39.4	23.6
Solvent	31.3	28.4	32.2
Ramachandran statistics[e]			
Preferred (%)	96.15	91.82	97.7
Allowed (%)	2.60	5.86	2.3
Root mean square deviation			
Bond lengths (Å)	0.008	0.029	0.015
Bond angles (°)	1.155	1.262	1.785
PDB entry	4OFC	4IH3	4IGN

[a] Values in parentheses are for the highest resolution shell.

[b] $R_{merge} = \Sigma_i |I_{hkl,i} - \langle I_{hkl} \rangle| / \Sigma_{hkl} \Sigma_i I_{hkl,i}$, where $I_{hkl,i}$ is the observed intensity and $\langle I_{hkl} \rangle$ is the average intensity of multiple measurements.

[c] $R_{work} = \Sigma||F_o|-|F_c||/\Sigma|F_o|$, where $|F_o|$ is the observed structure factor amplitude, and $|F_c|$ is the calculated structure factor amplitude.

[d] R_{free} is the *R* factor based on 5% of the data excluded from refinement.

[e] Based on values attained from refinement validation options in COOT.